Magnetic State of Multilayered Synthetic Antiferromagnets during Soliton Nucleation and Propagation for Vertical Data Transfer

Amalio Fernández-Pacheco, Nina-Juliane Steinke,* Dishant Mahendru, Alexander Welbourne, Rhodri Mansell, Shin L. Chin, Dorothée Petit, JiHyun Lee, Robert Dalgliesh, Sean Langridge, and Russell P. Cowburn*

Magnetic solitons in multilayered synthetic antiferromagnets (SAFs) have been recently proposed as data carriers for vertical data transfer, constituting a promising approach for 3D spintronic systems. Here, the nucleation and propagation of solitons in CoFeB/Ru SAFs are investigated under external magnetic fields by magnetooptical Kerr effect (MOKE), magnetoresistance (MR), and polarized neutron reflectivity (PNR) measurements. By comparing MOKE and MR measurements with macrospin simulations, the key steps of the mechanism behind soliton nucleation, triggered by the surface spin-flop transition and involving the switching of several layers, are determined. PNR confirms this scenario, and proves the correct propagation of solitons, with their expulsion leading to data inversion (NOT gate functionality). Additionally, the structure of solitons after nucleation is determined, finding them to be achiral under external magnetic fields.

1. Introduction

The transport of information in the form of solitons in coupled magnetic nanostructures[1] has made possible the development of an area of spintronics research known as nanomagnetic logic (NML).[2] The core idea of NML consists of using chains of coupled nanomagnets to transfer the magnetic state stored on a magnet at one edge of the chain to the other edge via dipolar interactions. This not only permits the transfer of magnetic data, but also allows complex sequential logic operations using logic gates to be performed.[3] The nonvolatility of this technology,[1] its potential ultra-low power consumption,[4] the possibility to address data using spin-transfer-torque[5] or the spin-Hall effect,[6] the robustness of some designs against data transfer errors caused by thermal fluctuations,[7] and the high speeds of data transfer[8] have identified NML as a promising candidate for future computing technologies. One of the main unresolved challenges for NML-based technology is data transfer in the vertical direction, a necessary step toward 3D spintronic systems.[9] We have recently extended the idea of using solitons in coupled magnets for vertical (out-of-plane) data transfer.[10–17] For this, multilayered synthetic antiferromagnets (SAFs) formed by N ferromagnetic layers and coupled via Rudderman–Kittel–Kasuya–Yosida (RKKY) interactions through $N-1$ nonmagnetic interlayers were used (**Figure 1**). We have shown that in an even-N-layer system, we can control the nucleation and propagation of solitons by exploiting the surface spin-flop transition (SSF):[10] an edge layer thicker than the others acts as a gate, switching independently from the rest at the SSF field and nucleating a soliton at the bottom of the system. When the field is relaxed, the RKKY coupling between layers causes the upper layers to switch in a cascade-like manner, propagating the soliton upward throughout the spin interconnector until it gets expelled. The final state at remanence is the contrary antiparallel state than at the start, a consequence of all layers switching, including the top output layer where information is read. This data transfer is analogous to some previously reported NML schemes,[1,2] but in this case along the vertical direction. Using perpendicularly magnetized (Ising) SAFs, it has also been shown that the propagation of solitons can be performed synchronously with an external magnetic field when the properties of the SAF are tuned in a ratchet fashion, with the system acting as a soliton shift register.[14,15,17] In this work, we explore in detail the behavior of SAFs under external magnetic fields during soliton nucleation and asynchronous propagation[10,13] by using the Kerr effect, magnetoresistance, polarized neutron reflectivity (PNR) measurements, and macrospin simulations.

Dr. A. Fernández-Pacheco, Dr. D. Mahendru, A. Welbourne, Dr. R. Mansell, Dr. S. L. Chin, Dr. D. Petit, Dr. J. H. Lee, Prof. R. P. Cowburn
Cavendish Laboratory
University of Cambridge
JJ Thomson Avenue, Cambridge CB3 0HE, UK
E-mail: af457@cam.ac.uk

Dr. N.-J. Steinke, Dr. R. Dalgliesh, Prof. S. Langridge
ISIS Neutron Source
Rutherford Appleton Laboratory
Oxon OX11 0QX, UK
E-mail: nina-juliane.steinke@stfc.ac.uk

DOI: 10.1002/admi.201600097

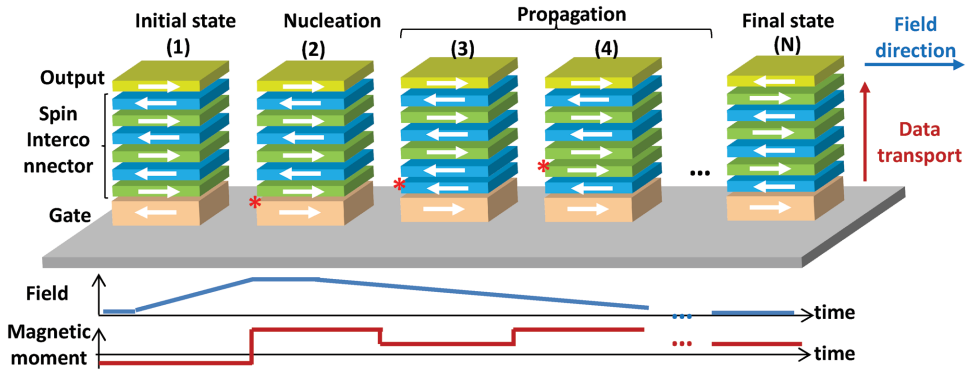

Figure 1. Data operation based on the vertical motion of solitons in multilayered SAFs. The top part of the figure shows schematically the types of systems used and the bottom part shows the field sequence and the magnetic moment of the SAF during soliton motion. Following a well-defined initial state at zero fields (1), with all layers antiparallel to each other, the field is increased up to a value where a soliton is nucleated at the bottom of the system, by the switching of the gate layer (2). After this, the field is reduced, propagating the soliton upwards (3, 4, ...), until it is expelled, reaching the final state (*N*).

The combination of all these techniques and simulations allows us to resolve the magnetic sates of the system during vertical data transfer, finding that the nucleation process is more complex than expected, via the switching of multiple layers, and this is followed by a correct soliton propagation and expulsion.

2. Results and Discussion

2.1. Soliton Nucleation

The SAFs are formed by CoFeB/Ru multilayers, with N ferromagnetic CoFeB layers, separated by $N-1$ Ru spacers. In particular, we have studied systems with $N = 4$ and 6, where the soliton nucleation and propagation mechanisms are equivalent. The samples were studied by applying external magnetic fields and electrical currents along the easy axis (EA), simultaneously measuring longitudinal magneto-optical Kerr effect (MOKE) and magnetoresistance (MR) signals. The MR measurements were performed using a van der Pauw configuration. **Figure 2**a shows the experimental major loop MOKE signal for an $N = 4$ SAF: coming from negative saturation (state I), the system transitions into a well-defined remanent state, formed by antiparallel spins, with the bottom gate layer pointing left (state II). This is the initial state of operation. As the field

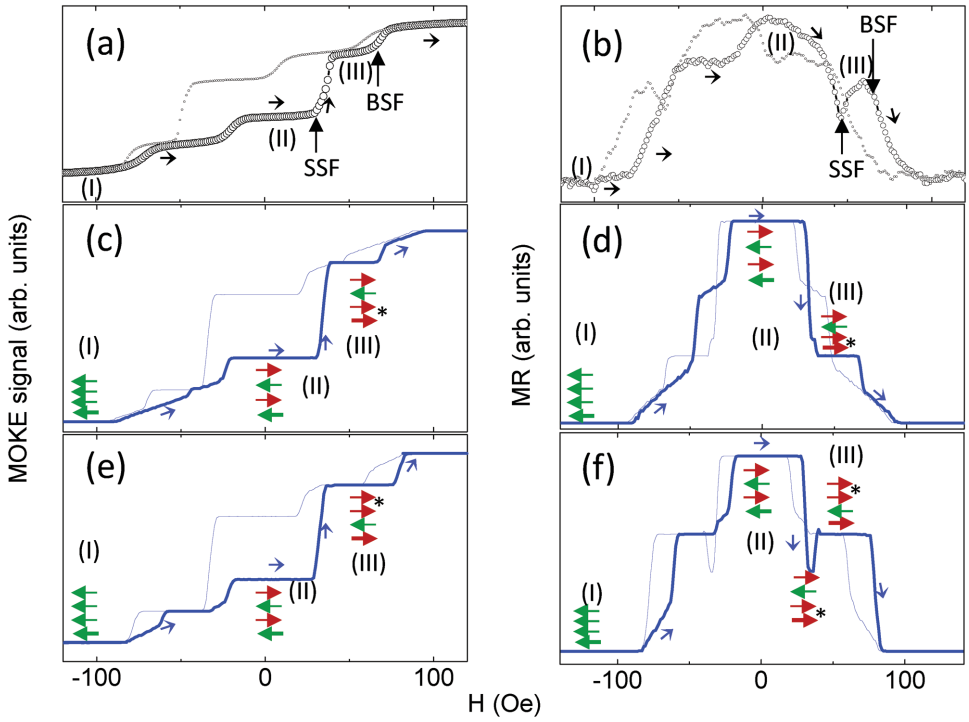

Figure 2. MOKE and MR in an $N = 4$ SAF. a,b) The figure shows experiments and different simulations with two sets of parameters. c,d) All layers have the same properties, whereas in panels (e) and (f) the first interface has a higher RKKY coupling than the others. The arrows in the figures show the magnetic state of the SAF as extracted from the simulations, for the three states explained in the text (I, II, and III). The asterisk indicates the position of the soliton in the system. A good agreement is obtained between experiments (panels (a) and (b)) and the second set of simulations (panels (e) and (f)).

becomes positive, the system transits at the SSF field: $H_{SSF} = (2H_{J1}H_{u1} + H_{u1}^2)^{1/2} \approx 30$ Oe, nucleating a soliton, as a consequence of the gate layer switching (state III). Here H_{Ji} and H_{ui} refer to the coupling and anisotropy fields of layer i, respectively (see the Experimental Section for details). These two states correspond to the first two steps of Figure 1 (for $N = 4$). If higher positive fields are applied, the soliton is erased, as a consequence of all the layers flopping toward the field, at the bulk spin-flop transition (BSF): $H_{BSF} = (4H_J H_u + H_u^2)^{1/2} \approx 60$ Oe. Figure 2b shows the corresponding MR measurements, with the same states marked as before. The MR signal is dominated by the Giant Magnetoresistance (GMR) effect, which decreases as the system goes from antiparallel alignment at remanence to saturation. A slightly larger field dispersion during switching is observed in MR in comparison with MOKE measurements. This is a consequence of the different areas probed by the two techniques (the MOKE laser spot has a ≈ 5 μm diameter, and the MR measurements are carried out on a 0.5×0.5 cm^2 square sample).

In order to fully understand the behavior of the SAF during soliton nucleation, we compare experiments with MOKE and MR signals obtained from macrospin simulations. Figure 2c,d shows simulated signals for an SAF with identical anisotropy and coupling values for all layers. The MOKE signal extracted from simulations is in good agreement with the experimental one; this is also the case for vibrating sample magnetometry measurements (see the Supporting Information). The corresponding simulated MR (Figure 2d) reproduces most features observed experimentally (Figure 2b). However, it does not reproduce the kink observed in experiments near the SSF transition. In order to understand this feature, we have simulated different SAFs where the properties of each layer are allowed to vary. Figure 2e,f shows MOKE and MR measurements for a system with same anisotropy H_u for all layers, but where the coupling value J has been increased by 15% for the bottom layer, and decreased by 10% for all the other layers (see the details in the Supporting Information). This has a significant effect on the magnetic behavior of the system during soliton nucleation: similarly, to the "homogeneous" system simulated before, a soliton is nucleated at the bottom of the system at the SSF. But in the other case the soliton is stable located at the bottom; here, due to the larger coupling at the first interface, it is almost immediately moved upward, reaching the third interface (see the arrows in Figure 2f), where it remains until the BSF field is reached. In this case, both MOKE and MR simulated signals agree well with the experimental ones. It is important to note that the overall magnetic moment of the SAF is the same when a soliton formed by two layers pointing right is located either at the bottom or at the top of the system. Both states are therefore indistinguishable with bulk magnetometry measurements and very difficult to identify with MOKE due to the complex magneto-optical response of multilayered systems.[18] However, as the bottom gate layer is three times thicker than the rest, higher current will flow through it, dominating the MR signal. Therefore, the resistance of the system is smaller if a soliton is located at the first interface than if it is located at any other, due to the GMR contribution to the total MR of the system. The kink around the SSF therefore appears to be the result of soliton nucleation via switching of the gate layer at the SSF transition (decrease of MR when layers 1–2 become parallel), followed by immediate soliton partial propagation (moderate increase of MR corresponding to parallel layers 3–4) for fields between the SSF and BSF.

In order to confirm the interpretation derived from MR measurements, we have performed experiments using PNR, a layer-resolved magnetometry technique. Using the in situ MOKE system at the beamline, PNR measurements were performed at well-defined magnetic states and correlated with MOKE and MR results. **Figure 3** shows experimental data and fits for an $N = 4$ SAF similar to the one previously described. Only nonspin-flip channels are shown, since the signal measured in the spin-flip channels was negligible. The lack of off-specular signal for the states investigated indicates no significant domain formation within the length scales PNR is sensitive to, justifying the macrospin approach presented here. This also indicates that the magnetization was always found to be along the EA for any of the magnetic states investigated, i.e., any soliton in the system was found to be sharp (achiral), with no deviation of the magnetization from the EA. This contrasts with previous results where PNR was used to investigate the magnetic state of Fe/Cr multilayered SAFs, and where a strong deviation from the EA for layers forming wide solitons was detected.[19] A much larger H_J/H_u value in their case explains the remarkable difference with our results.[13]

The three magnetic states investigated are state I: saturation (Figure 3a), state II: remanence after saturation (Figure 3b), and state III: soliton nucleation after the SSF (Figure 3c,d). Fits were carried out using the GenX package.[20] The fits to the data were performed by tying the properties of all Ru and CoFeB layers, respectively, except for the thicker CoFeB gate layer, which reduces the number of free parameters (see the Supporting Information for details of the model). State I was used to extract the structural contribution and saturation magnetization. Figure 3b shows the best fit to state II, corresponding to the layers antiparallel to each other, with the bottom layer parallel to the negative field direction; this is the expected magnetic configuration, confirming a well-defined state as a starting point for soliton operation. Figure 3c,d shows the same experimental data, corresponding to state III. Several possible magnetic configurations were tested; here we show the two most relevant. In Figure 3c, a sharp soliton is assumed at the bottom, whereas in Figure 3d, a sharp soliton is assumed at the top. As observed, a good fit is obtained for a magnetic configuration with a sharp soliton at the top of the stack, but not at the bottom: PNR results are therefore in good agreement with the scenario previously described by MR and simulations, where the SAF was assumed to have higher coupling at the first interface. The combination of magnetometry, MR, and PNR measurements allows us to fully understand the magnetic state of the system during soliton nucleation.

2.1. Soliton Propagation

After the nucleation of a soliton at the SSF transition, the soliton is propagated by reducing the field until a second remanent state is reached. The soliton should move upward and be expelled from the system, resulting in the opposite antiparallel

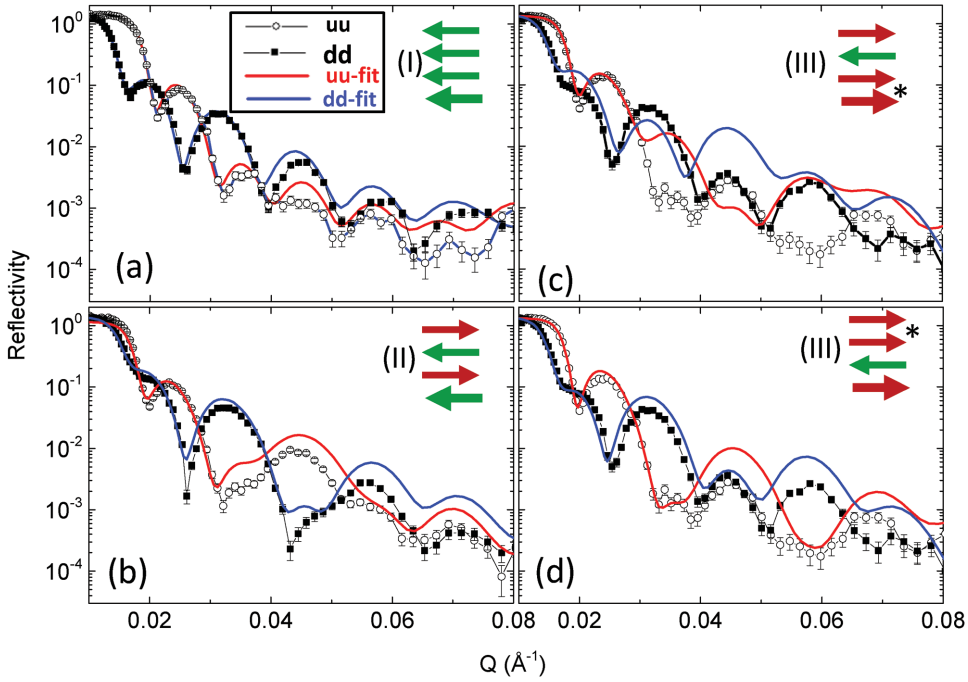

Figure 3. PNR experiments in an $N = 4$ SAF for the three states discussed in the text, corresponding to a) I: negative saturation, b) II: remanence after negative saturation, c,d) and III: state after the SSF transition. In the latter case, there is a better fit to the data when a soliton is formed by layers 3–4 than by 1–2 (panel (c)).

state (see the final state in Figure 1). We have investigated this process in an $N = 6$ SAF, where **Figure 4**a,b shows experimental MOKE and MR measurements and Figure 4c,d are the corresponding numerical signals from simulations. In light of the previous conclusions, the system was modelled with a slightly larger coupling between layers 1 and 2 than for the other interfaces (Supporting Information). Blue (black) dots and lines correspond to minor (major) loops. The arrows indicate the magnetic configuration for four states (I–IV), extracted from simulations.

Additionally, **Figure 5**a–f shows PNR data measured for these magnetic states with the best-fit magnetic configurations indicated. PNR fitting was carried out as previously discussed. As before, the kink in MR after the SSF indicates that the soliton is nucleated at the bottom, followed by partial upward propagation. Figure 5e shows how the best fit to the PNR data after the SSF occurs when a sharp soliton is located at layers 3–4, in comparison with fits assuming it to be placed at the top, formed by layers 5–6 (Figure 5d), or at the bottom, formed by layers 1–2 (Figure 5f). The simulated MR signal agrees well with this scenario.

After the SSF transition and with the soliton located in the middle of the system, the field is progressively reduced to zero in order to propagate the soliton upward, until reaching state IV. MOKE measurements (Figure 4a) show that the signal at this state is the same as at remanence for the other branch of the major loop, indicating that we have reached the opposite antiparallel state (IV is the mirrored state of II); PNR confirms this hypothesis, as shown in Figure 5c. We attempted to observe the soliton propagation under decreasing fields in more detail (from state III to state IV) using PNR, but we could not observe any intermediate state (soliton located between layers 4 and 5 or 5 and 6) before expulsion. Experimental and simulated MOKE and MR measurements show how the signals remain approximately constant for most of that field range, with an abrupt change only close to zero fields. In simulations, the soliton is sequentially propagated from the middle, step-by-step, until being expelled, at the same time that its width increases as the fields become lower. However, this process takes place over a very small range of fields in this system, which prevents the direct observation of intermediate states. In an SAF with an H_J/H_u ratio closer to 1 this should be possible.[13,16]

3. Conclusion

In summary, we have investigated the nucleation and propagation process of CoFeB/Ru SAFs with up to six layers under external magnetic fields, using simultaneous MOKE and MR measurements, macrospin simulations, and PNR. We have shown how in-plane MR is sensitive to the soliton position, differentiating states which are undistinguishable in other magnetometry measurements. This is an important step for future studies in patterned SAFs. MR measurements have made possible the detection of a complex soliton nucleation process, where the bottom gate layer switches at the SSF transition, followed by almost immediate partial propagation through the collective switching of nearby upper layers. In order to reproduce this process using macrospin simulations, we have modelled the system with a higher antiferromagnetic coupling at the first interface. The process reported here is a common issue in NML operation, where the switching of nanomagnetic bits is very sensitive to small variations in coupling between them.[1,2,21] In

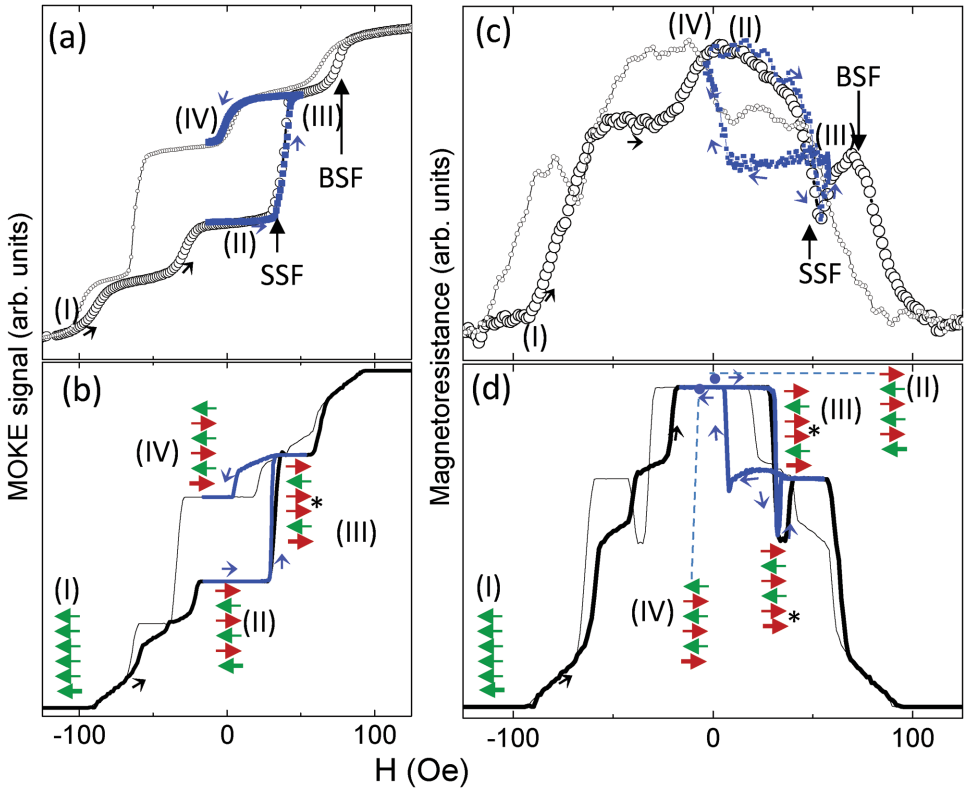

Figure 4. a,b) Experimental and c,d) simulated MOKE and MR measurements for an $N = 6$ SAF. The black dots and lines correspond to major loops, and the blue ones to minor loops. The arrows in the simulations show the magnetic state of the system extracted from simulations for the states discussed in the text (I, II, III, and IV).

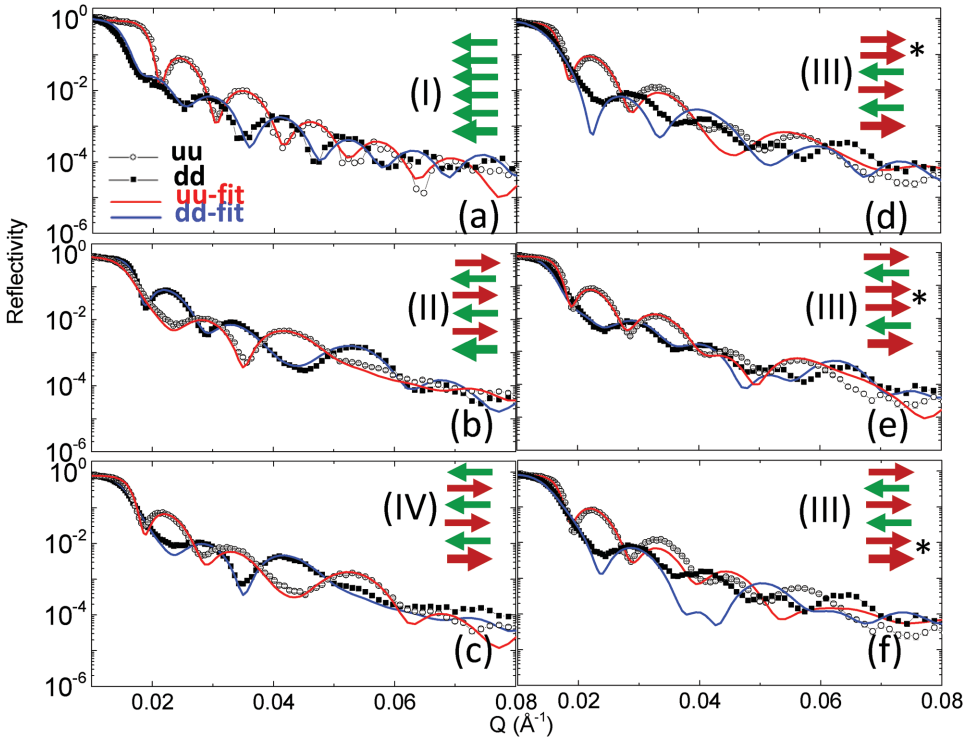

Figure 5. PNR experiments in an $N = 6$ SAF for the four states discussed in the text, corresponding to a) I: negative saturation, b) II: remanence after negative saturation, c) III: state after the SSF transition, d–f) IV: remanence after the SSF (panel (c)). In III, a better fit to the data is obtained when a soliton is formed by layers 3–4 (panel (e)) than by 5–6 (panel (d)) or 1–2 (panel (f)).

our case, according to the fits of PNR data, the bottom layer has smaller roughness than the rest of the layers (Supporting Information). The reasons behind this can be manifold:[22] different microstructures of underlying layers, variations in process pressure during growth, the dependence of roughness on layer thickness, and so on. These factors will result in different effective RKKY coupling values, which depend on orange-peel coupling and pinhole densities.[23]

The macrospin approach followed here adequately captures the overall behavior of the system for soliton nucleation, and describes correctly the initial and final states at both sides of the SSF transition. However, it cannot reproduce the exact details of the magnetization during the SSF, where the actual mechanism for the reversal of the layers, via nucleation and propagation of domains, is manifested. In particular, the macrospin approximation will fail if the reversal occurs via coupled domains between layers, which may be the case in unpatterned samples as those studied here. Supporting Information includes soliton stability measurements where the nonmacrospin behavior of the layers during switching is evidenced.

Finally, we have investigated the magnetic configuration of the stable states present during soliton operation using PNR measurements. PNR data allow us to determine the soliton position in the system, confirming the complex nucleation process inferred from MR and simulations, and demonstrates an inversion (NOT) signal operation, with the final antiparallel state resulting from soliton propagation, rather than the flopping of all layers at the BSF transition. Moreover, PNR resolves the magnetic structure of solitons during operation, finding them to be sharp (achiral), with the two layers forming the soliton pointing along the magnetic field. Future studies in SAFs with lower H_J/H_u coupling ratios could allow the observation of intermediate states during soliton propagation, stabilized by external fields, as well as chiral solitons at remanence, susceptible to move bi-directionally under rotating magnetic fields.[16]

4. Experimental Section

Sample Growth: The films were grown by magnetron sputtering at room temperature, with a base pressure of 5×10^{-8} mbar. Two substrates, either Si (001) with a native oxide or with 300 nm thermally oxidized SiO_x to perform electrical measurements, were used. A 4 nm Ta seed layer was added to improve the growth quality. The nominal CoFeB thicknesses were $t_1 = 15$ nm for the first (bottom) gate layer and $t = 5$ nm for the others (spin interconnector and top output). A field of several kOe was applied in-plane during growth in order to create a well-defined EA along the field direction, with anisotropy fields for the CoFeB layers $H_u \approx 20$ Oe.[10] The nominal Ru thickness was 3.5 nm (third RKKY antiferromagnetic peak), corresponding to a coupling value of $J \approx -20$ merg cm^{-2}.[10] The coupling fields were therefore $H_J = |J|/M_s t \approx 34$ Oe and $H_{J1} = |J|/M_s t_1 \approx 10$ Oe for the layers forming the spin interconnector and the bottom gate layer, respectively (the saturation magnetization of CoFeB, $M_s = 1200$ emu cm^{-3}, was determined by vibrating sample magnetometry). For the spin interconnector, the coupling/anisotropy ratio of those layers fulfilled $H_J/H_u > 1$, which was a necessary condition to obtain an antiparallel state at remanence and to propagate solitons along the system.[10,13]

Magnetoresistance Measurements: Room temperature current-in-plane magnetoresistance measurements were carried out in the van der Pauw configuration. Simultaneous MOKE and MR measurements were performed in a longitudinal configuration, by applying external magnetic fields and electrical currents along the EA.[24] The behavior of the system using Monte Carlo macrospin simulations was modelled: each layer in the system was equivalent to a single (macro) spin, which reversed by rotating under external magnetic fields. By comparing the associated magnetic moment and MOKE signal from simulations with the experimental results, the properties of the SAF under study can be extracted.[10]

Magnetoresistance Modelling: The MR for the (CoFeB/Ru) multilayer was computed using the magnetic state for each field value obtained from simulations. For this, the electrical signal was modelled as the one associated with a resistor system formed of N parallel resistors for the Anisotropic Magnetoresistance (AMR) contribution, in series with $N - 1$ parallel resistors for the GMR contribution, with the appropriate values for both contributions extracted from comparison with experimental results[25] (see the Supporting Information for details of the model).

Polarized Neutron Reflectometry: PNR measurements were carried out at the OffSpec reflectometer at the ISIS neutron and muon source. During the measurements an in-plane magnetic field along the EA of the sample and parallel to the quantization axis of the neutron spin was applied. Transverse MOKE measurements were carried out in situ immediately before and after the neutron measurements. Using the hysteresis loops, it was possible to precisely control the magnetic state of the sample for the neutron measurements.

Supporting Information

Supporting Information is available from the Wiley Online Library or from the author.

Acknowledgements

This work was funded by EPSRC, including an EPSRC Early Career Fellowship EP/M008517/1, by the Winton Foundation, and by the European Community under the Seventh Framework Programme Contract No. 247368, 3SPIN. Experiments at the ISIS Pulsed Neutron and Muon Source were supported by a beamtime allocation from the Science and Technology Facilities Council.

Received: February 3, 2016
Revised: April 11, 2016
Published online: May 9, 2016

[1] R. P. Cowburn, M. E. Welland, *Science* **2000**, *287*, 1466.
[2] M. T. Niemier, G. H. Bernstein, G. Csaba, A. Dingler, X. S. Hu, S. Kurtz, S. Liu, J. Nahas, W. Porod, M. Siddiq, E. Varga, *J. Phys. Condens. Matter* **2011**, *23*, 493202.
[3] A. Imre, G. Csaba, L. Ji, A. Orlov, G. H. Bernstein, W. Porod, *Science* **2006**, *311*, 205.
[4] B. Lambson, D. Carlton, J. Bokor, *Phys. Rev. Lett.* **2011**, *107*, 010604.
[5] A. Lyle, J. Harms, T. Klein, A. Lentsch, D. Martens, A. Klemm, J.-P. Wang, *Appl. Phys. Lett.* **2012**, *100*, 012402.
[6] D. Bhowmik, L. You, S. Salahuddin, *Nat. Nanotechnol.* **2014**, *9*, 59.
[7] D. B. Carlton, N. C. Emley, E. Tuchfeld, J. Bokor, *Nano Lett.* **2008**, *8*, 4173.
[8] Z. Gu, M. E. Nowakowski, D. B. Carlton, R. Storz, M.-Y. Im, J. Hong, W. Chao, B. Lambson, P. Bennett, M. T. Alam, M. A. Marcus, A. Doran, A. Young, A. Scholl, P. Fischer, J. Bokor, *Nat. Commun.* **2015**, *6*, 6466.

[9] R. L. Stamps, S. Breitkreutz, J. Åkerman, A. V. Chumak, Y. Otani, G. E. W. Bauer, J.-U. Thiele, M. Bowen, S. A. Majetich, M. Kläui, I. L. Prejbeanu, B. Dieny, N. M. Dempsey, B. Hillebrands, *J. Phys. D: Appl. Phys.* **2014**, *47*, 333001.
[10] A. Fernández-Pacheco, D. Petit, R. Mansell, R. Lavrijsen, J. H. Lee, R. P. Cowburn, *Phys. Rev. B: Condens. Matter Mater. Phys.* **2012**, *86*, 104422.
[11] J. H. Lee, D. Petit, R. Lavrijsen, A. Fernández-Pacheco, R. Mansell, R. P. Cowburn, *Appl. Phys. Lett.* **2014**, *104*, 232404.
[12] J.-H. Lee, R. Mansell, D. Petit, A. Fernández-Pacheco, R. Lavrijsen, R. P. Cowburn, *SPIN* **2013**, *03*, 1340013.
[13] A. Fernández-Pacheco, R. Mansell, D. Mahendru, A. Welbourne, J. H. Lee, S.-L. Chin, D. Petit, R. P. Cowburn, in *Topological Structures in Ferroic Materials* (Ed: Jan Seidel), Springer International Publishing, Cham, Switzerland, **2016**.
[14] R. Mansell, R. Lavrijsen, A. Fernández-Pacheco, D. C. M. C. Petit, J. H. Lee, B. Koopmans, H. J. M. Swagten, R. P. Cowburn, *Appl. Phys. Lett.* **2015**, *106*, 092404.
[15] R. Lavrijsen, J.-H. Lee, A. Fernández-Pacheco, D. C. M. C. Petit, R. Mansell, R. P. Cowburn, *Nature* **2013**, *493*, 647.
[16] D. Petit, R. Mansell, A. Fernández-Pacheco, J. H. Lee, R. P. Cowburn, in *VLSI Circuits for Emerging Applications* (Ed: T. Wojcicki), CRC Press, Boca Raton, FL **2014**.
[17] R. Lavrijsen, D. C. M. C. Petit, A. Fernández-Pacheco, J. Lee, M. Mansell, R. P. Cowburn, *Nanotechnology* **2014**, *25*, 105201.
[18] J. Hamrle, M. Nývlt, Š. Višňovský, R. Urban, P. Beauvillain, R. Mégy, J. Ferré, L. Polerecký, D. Renard, *Phys. Rev. B* **2001**, *64*, 155405.
[19] S. te Velthuis, J. Jiang, S. Bader, G. Felcher, *Phys. Rev. Lett.* **2002**, *89*, 127203.
[20] http://genx.sourceforge.net/, **2016**.
[21] B. Lambson, Z. Gu, D. Carlton, S. Dhuey, A. Scholl, A. Doran, A. Young, J. Bokor, *Appl. Phys. Lett.* **2012**, *100*, 152406.
[22] E. Fullerton, D. Kelly, J. Guimpel, I. Schuller, Y. Bruynseraede, *Phys. Rev. Lett.* **1992**, *68*, 859.
[23] *Nanomagnetism: Ultrathin Films, Multilayers and Nanostructures*, Elsevier, Amsterdam, The Netherlands, **2006**.
[24] H. T. Zeng, D. Read, D. Petit, A. V. Jausovec, L. O'Brien, E. R. Lewis, R. P. Cowburn, *Appl. Phys. Lett.* **2009**, *94*, 103113.
[25] T. Charlton, D. Lederman, G. P. Felcher, *MRS Proc.* **2011**, *674*, T1.4.

